Evaluation of adaptive algorithms for detection and classification of fluorescent aerosols in the atmosphere

Pierre Lahaie, Jean-Robert Simard and Sylvie Buteau, DRDC Valcartier, 2459 de la Bravoure Road Québec, Québec G3J 1X5 CANADA

Abstract

Photon counting technologies are developed and could be used in the future to measure the return from laser induced fluorescence. Currently, the spectral detection of light emitted by fluorescing aerosols is performed with ICCD, Intensified Charge Coupled Device. The signal to noise ratio of ICCD devices is smaller by a factor of $\sqrt{2}$ compared to photon counting devices having the same sensitivity. We studied the impact of this difference of signal to noise ratio on the capability of multivariate detection and classification algorithms to operate on various conditions. Signal simulations have been performed to obtain ROC (Receiver Operation Characteristics) Curves and Confusion Matrix to obtain the detection performance and the ability of algorithms to discriminate a potential source from another. Two detection algorithms are used, the Integrated Laser Induced Fluorescence (ILIF) and the Matched Filter. For the classification, three algorithms are used, the Adaptive Matched Filter (AMF), the Adaptive Coherent Estimator (ACE) and the Adaptive Least Squares (ALS). The best algorithm for detection is the AMF using the signature of the material present in a cloud, the ILIF detector performs very well. For the classification, the three algorithms are surprisingly giving the same results for the same data. The classification performs better if the distance between the signatures recorded in a database is important. The performance of the detector and of the classificator improves with an increase of the signal to noise ratio and is consistently and significantly better for the photon counting compared to ICCD.

Keywords : Fluorescence, spectra, multivariate, algorithm, detection, classification.

1. Introduction

Future trends in detector development provide the possibility that High Speed High Intensity Photon Counting Sensor (HSHIPCS) be available in the future for spectral detection in Lidar remote sensing [1]. These devices will be very attractive for the detection of fluorescent aerosol contaminants in the atmosphere because of the large signal to noise ratio they provide under very small signal regime. This paper focuses on the advantages that such a detector will provide when compared to ICCD (Intensified charge coupled device) which are presently state of the art, operated in analog mode. Among a larger signal to noise ratio, HSHIPCS will enable the acquisition of a spectral map of the fluorescent aerosols, by scanning the area surrounding the sensor, a feature that cannot be delivered by ICCD since they are gated devices.

In this paper, we compare the performance for detection and classification of two detectors operated in the same optical system and having as their only difference the fact that the ICCD is operated in analog mode and another detector operated in photon counting mode. The results are fed to detection and classification algorithms. The only difference is the noise model used for the ICCD and for the HSHIPC. For both detectors, the input signal is considered to be Poisson shot noise. Since the quantum efficiency is the same, the HSHIPCS keeps the signal as it is and the ICCD signal is modified to account for the randomness of the multiplication process [2].

The selected detection and classification algorithms are ACE [4](Adaptive correlation estimator), AMF [3] (Adaptive matched filter) based on the GLRT [5](Generalized likelihood ratio test) that have originally been developed for processing of radar data and hyperspectral imagery. The assumptions supporting their development are that only the background contributes to the clutter and the only noise source is the sensor. In the case of hyperspectral detector, the optical signal is larger than for fluorescence detection. The electronic noise of these sensors can be larger than the shot noise, a Gaussian approximation can be used for the noise in that case. For fluorescence spectral sensors, the signal is much lower and the sensors are limited by photon shot noise. The clutter characteristics may not show a large correlation between spectral bands and moreover the noise level varies with the signal level. These facts make the assumptions behind the AMF and ACE algorithms to be broken. Another algorithm ALS for Adaptive least Square is added to the set of evaluated algorithms. In the paper, we describe first the signal, then we succinctly describe the algorithms. The

algorithms' performances are evaluated through the use of Monte-Carlo simulations. The results are presented as ROC (Receiver Operating Characteristic) curve for detection and confusion matrix for classification.

2. Signal model

The model for a single band is derived from the contribution of background fluorescing aerosol signal having a mean $\langle x \rangle$ and contaminating aerosols having a signature *s* and noise from the sensor. The model for the mean of the signal is given by equation (1), where *r* is the mean of the measured signal, *x* is the mean of the background, *s* is the contaminant's spectral signature and α is a number proportional to the concentration of the contaminant, the signature content. We first discuss the noise, then the background and finally the signatures.

$$\langle r \rangle = \langle x \rangle + \alpha s \tag{1}$$

For the photon counting detector, the mean and the variance of the signal are the same and therefore a measured signal would have the following form where *N* is the noise due to the random arrival of photons:

$$r = \langle x \rangle + \alpha s + N \tag{2}$$

The expectation value for the noise is null and the variance is the same as the mean for Poisson shot noise:

$$\sigma_r^2 = \langle x \rangle + \alpha s \tag{3}$$

We assume that the covariance between spectral channels is null because the probability to receive two photons from the same particle and the same laser pulse is very small and it is the only mechanism for correlation if the background is stationary (particle concentration and nature do not change). Photon shot noise also reduces the possibility for correlation by a large amount since the random arrival of photons is independent from a channel to another. If the statistics of the background evolve with time, extra diagonal elements in a covariance matrix will grow. The situation can remain stationary in the wide sense if the statistics of the background do not change with time.

ICCD detectors are made of a photocathode cascading on a microchannel plate, a phosphor plate and a CCD (Charge Coupled Device) detector. The photocathode detects a photon and produces an electron. It is characterized by its quantum efficiency which is the probability that a photon produces an electron. We assume that this detection probability is the same for the photon counting device and for the ICCD. The microchannel plate amplifies the signal by multiplying the original electron with a random number of electrons. This random number is according to [5] modeled with an exponential distribution. Another source of noise in the ICCD originates from the dark current noise. This noise source is neglected in this study because if the detector and sampler are well designed its value can be smaller than the sampling interval of the digitizer. The signal model for the ICCD is:

$$\langle r \rangle = G\langle x \rangle + G\alpha s \tag{4}$$

Where G is the gain of the ICCD. The signal can be modeled by:

$$r_{ICCD} = G\langle x \rangle + G\alpha s + N_{ICCD} \tag{5}$$

The variance of the noise is accordingly to [2] increased by a factor of 2 above the gain of the sensor. The signal to noise ratio (SNR) of the ICCD is degraded by a factor of $\sqrt{2}$ compared to the SNR of the photon counting device.

2.1 The background

The most general case for a background composed of fluorescent aerosols can be assumed to be a slowly varying signal around an average spectral shape. The variation and average will depend strongly on the area where the sensor is deployed. In urban area for example, the activity can generate fluorescent aerosols that could vary in time and nature depending on the level of activity or on the weather. The characteristics of these variations are largely unknown. The background that we selected is constant with time and generates variation only due to photon shot noise. The spectral shape is ad hoc, but is selected in such a way that it is not too close to the signatures composing the database. The spectral background selected is given in figure 1.

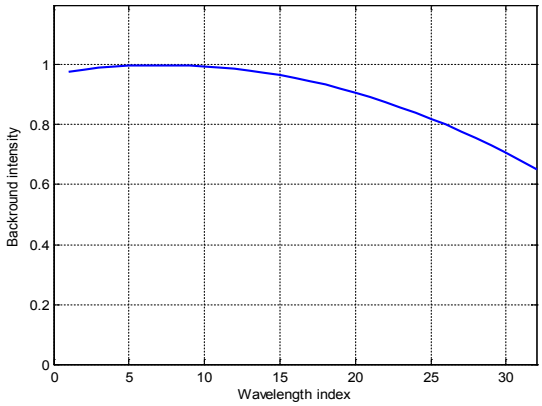

Figure 1: Spectral representation of the average of the background. The actual background used in the simulations has the same shape but is normalized to give a sum of 1.

2.2 The signatures

Signature of materials depends on their structure, chemical constituents, production process etc… The sources of signal production are fluorescent molecules and alteration sources for the spectrum are numerous and not well understood. It is important to maximize the signal to noise ratio to enable a system to see differences in a large number of possibilities and small differences between materials. In the literature, some measurements are available [6], [7], [8]. We are interested by fluorescence excitation from UV laser operated around 350 nm. The small amount of spectral features and the bulk appearance of the fluorescence spectrum make difficult the differentiation between spectra. Spectra are not orthogonal. The signatures set is shown in figure 2. They are analytic functions of the general form:

$$f_i(x) = (x-a)^2 \exp\left(-\frac{(x-b_i)^2}{c}\right) \quad (6)$$

In which $a = 1.1$, $c = 2$ and we have chosen 10 values for b_i extending from 2 to 3 in order that the Euclidean distance between adjacent functions be equal. This distance choice should provide a reference for the proximity of any two functions in a similar experiment.

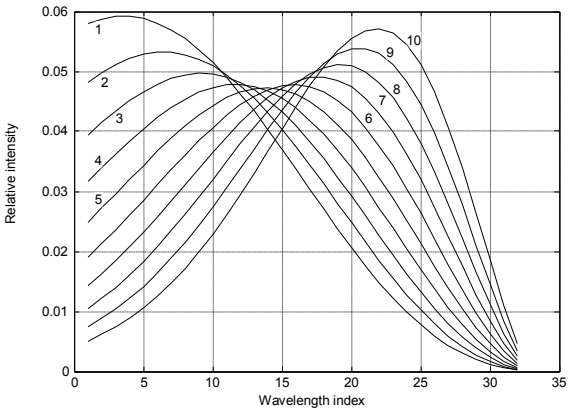

Figure 2: Signatures used in the simulations. The number close to each curve is the identifier.

3. Algorithms

There are two purposes for the algorithms: detection and classification. We consider that detection occurs when the signal departs significantly from the background. Classification is attempted when a departure from background happens. The algorithms that we propose in this study can be used mainly for classification. However, they can also, under some assumptions, be used to perform detection. Returning to the signal model of equation (1):

$$r = x + \alpha s \tag{7}$$

Remembering that we deal with vector quantities, a simple estimator for the signature content in the signal has the form:

$$\alpha = \frac{(r - \langle x \rangle)'.s}{s'.s} \tag{8}$$

Where the dot denotes the scalar product. The inclusion of material's signature accounts for the adaptive qualification of the filter. A linear filter in the form of a matrix can be inserted in the structure which gives:

$$\alpha = \frac{(r - \langle x \rangle)'.F.s}{s'.F.s} \tag{9}$$

This parameter does not give clue about the belonging of the measurement to a signature's class. To perform that, a distance or error estimator is required. We will derive the LS (Least Square) detector in the following and provide the results for the AMF and ACE detector. The estimators given in equation (8) and (9) can be used as detectors, since the output value will depart from 0 when the signal will increase. This is true for any signature selection because they are not orthogonal; however, a detector using a signature that is very close to the signature of the material generating the signal will be better than any other. Another detector used in the study is the integrated signal, called ILIF in the remaining of the paper, shown in equation (10) if *v* is a vector made of 1. Selective weighting can be used by modifying the vector *v* in the hope of reducing the noise.

$$\alpha = v'r \tag{10}$$

3.1 The Adaptive LS detector (ALS)

The error in the LS formalism is given by:

$$|E|^2 = \sum_S (r - \langle x \rangle - \alpha s)^2 \tag{11}$$

Where S is the spectral intervals. In vector notation it gives:

$$|E|^2 = (r - \langle x \rangle - \alpha s)'.(r - \langle x \rangle - \alpha s) \tag{12}$$

This gives:

$$|E|^2 = (r - \langle x \rangle)'.(r - \langle x \rangle) - 2\alpha(r - \langle x \rangle)'.s + \alpha^2 s'.s \tag{13}$$

Taking the derivative with respect to α and equating to 0 to minimize the error, yield:

$$\frac{d|E|^2}{d\alpha} = -2(r - \langle x \rangle)'.s + 2\alpha s'.s = 0 \tag{14}$$

When α is isolated, we obtain equation (8). Replacing α in equation (13) gives the ALS detector equation (15):

$$|E|^2 = (r - \langle x \rangle)'.(r - \langle x \rangle) - \frac{\left((r - \langle x \rangle)'.s\right)^2}{s'.s} \tag{15}$$

A linear filter can be introduced in the detector this gives a MALS (Modified Adaptive Least Square) detector:

$$|E|^2 = (r - \langle x \rangle)'.F.(r - \langle x \rangle) - \frac{((r - \langle x \rangle)'.F.s)^2}{s'.F.s} \tag{16}$$

The AMF detector is obtained through the maximum likelihood formalism with the assumption of a multivariate Gaussian distribution and the ACE detector assumes a T-Distribution with parameter 2. They use the same equation for the proportion of material in the measurement as the ALS, but the detectors are different and are given below:

$$D_{AMF}^2 = \frac{((r - \langle x \rangle)'.\Sigma^{-1}.s)^2}{s'.\Sigma^{-1}.s} \tag{17}$$

$$D_{ACE}^2 = \frac{((r - \langle x \rangle)'.\Sigma^{-1}.s)^2}{(r - \langle x \rangle)'\Sigma^{-1}(r - \langle x \rangle)s'.\Sigma^{-1}.s} \tag{18}$$

Where Σ is the covariance matrix assumed in the Gaussian component of the multivariate distribution. In case where the background data can be modeled with an elliptic distributions e.g. Gaussian, T, the inverse of the background covariance matrix provides very good results. In the case of the filter introduced in the MALS detector, no method exists to the author's knowledge to derive it, the inverse of the background covariance matrix can be used since it is the best operator to decorrelate (whitens) the background and minimize the variance due to the background clutter for elliptically symmetric distributions. In our case, the noise distribution is Poisson for the photon counting sensor and close to Poisson for the ICCD, it would be interesting to find a filter well adapted to optimize the performance of the detectors, but it is devoted to future work.

4. Simulations

The simulations are performed on the same photons signal. We first compute the Poisson shot noise for each channel of a spectrometer using a simple Poisson random number generator. The probability slots are computed using Poisson distribution, given by:

$$P(n) = \frac{e^{-\lambda}\lambda^n}{n!} \tag{19}$$

The list of probability values is: $\{P(n = 0), P(n \leq 1), P(n \leq 2), P(n \leq 3), P(n \leq 4), \ldots, P(n \leq \infty)\}$. Where $P(n \leq m) = \sum_{i=0}^{m} p(n = i)$. The generated random number is compared to the list and the value of n corresponds to the number of elements of the list that are below its value. This process is performed for each channels of the sensor. At this stage the signal is fed through the detection process standing for the photon counting detector. For the ICCD, we compute random exponential random variable for each photon. The process is, for N photons:

$$r = \sum_{n=1}^{N} -Gln(1 - F) \tag{20}$$

Where *F* is a random number respecting the uniform distribution function. It has this form because the exponential probability density is given by:

$$f_x(x) = \frac{1}{G} exp\left(-\frac{x}{G}\right) \tag{21}$$

And the probability distribution is:

$$F_x(x) = 1 - exp\left(-\frac{x}{G}\right) \tag{22}$$

The simulation for a single signal is performed using the following sequence given in figure 3.

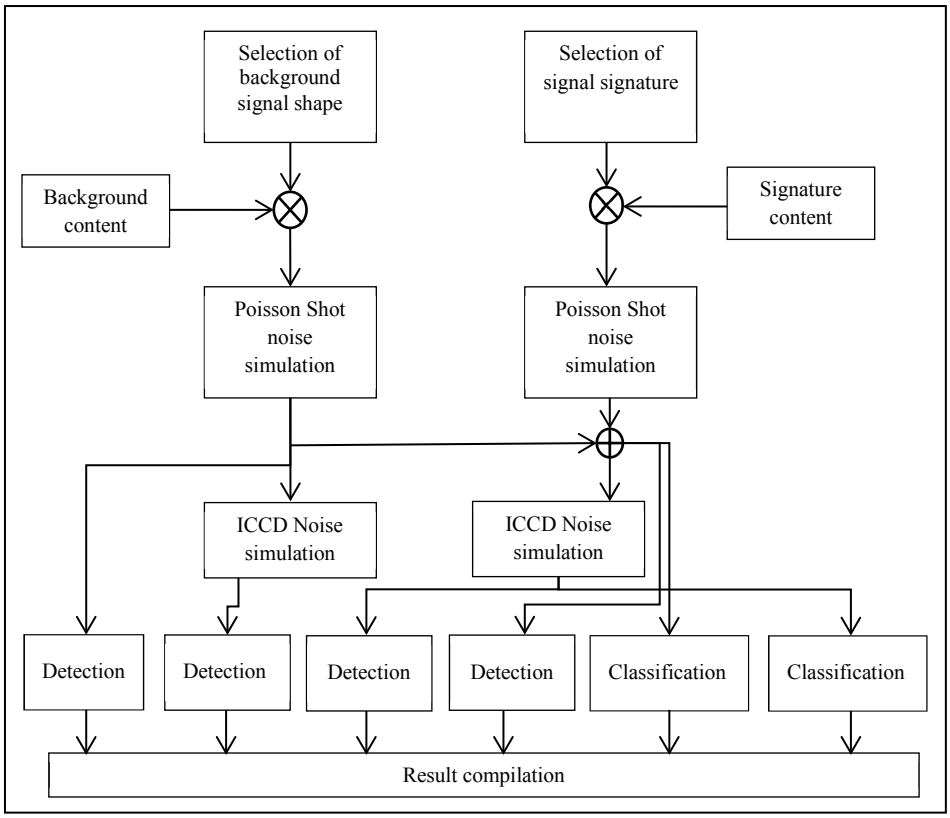

Figure 3: Simulation sequence

The different stages of the simulation have been discussed above. The signature and background contents are parameters that are used to respectively multiply the background and the signature functions in order to build the average of a signal in a given condition. The detection is the process by which a signal is classified as being part of the background or not. Classification is the process by which a signal for which detection has been positive and is used to find the signature that is the most probable. In this work, we are in closed set, meaning that a contaminated signal is generated with a contaminant existing in the database. We use three operators for the classification equations (16), (17) and (18) and two operators for the detection, equations (8) and (10). The covariance matrix is replaced with the unitary matrix.

5. Results

5.1 ROC curves

ROC curves have been obtained for conditions in which the background content or strength is 100 and the signature content or strength varies from 5 to 100. Each of these values (strength) multiplies the background and the signature the signal is the addition of the two results. Remember that the sum over the 32 channels of the function of the background and of the signature is unity. The thresholds list is computed from a probability of false alarm using only background measurements for obtaining the intervals. Figure 4 shows three graphs; the first one is the average of a signal having a signature content of 1000 for the fifth signature of figure 2 and a background content of 100; The second and third graphs report the same mean signal but with the injection of the noise signal following equations (19) (basic shot noise) and (21) (ICCD noise), respectively. Figure 5 displays ROC curve comparisons for the detection using for the ICCD and for the shot noise sensors the ILIF and the matched filter detectors for the different signatures inserted in the matched filter. Figure 6 shows the probability of detection for a constant probability of false alarm of $1x10^{-4}$ as a function of the signature content depending on the signature used to simulate the signal and the best detection for the 5^{th} signature.

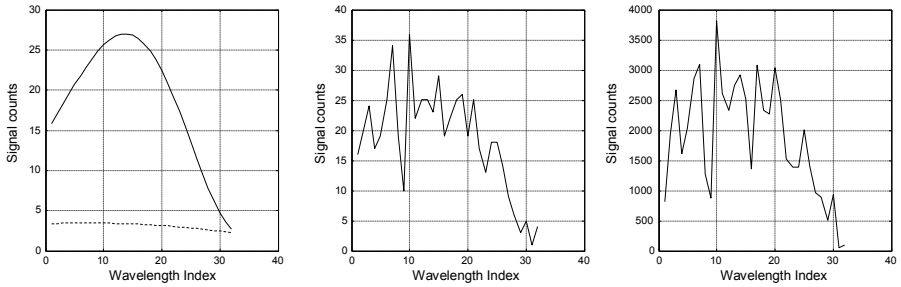

Figure 4: In the figure on the left, the average for the background (bottom dashed) and the signal. The center figure is a single realization of a shot noise acquisition and the figure on the right is the ICCD noise signals for background strength of 100 and signature strength of 1000.

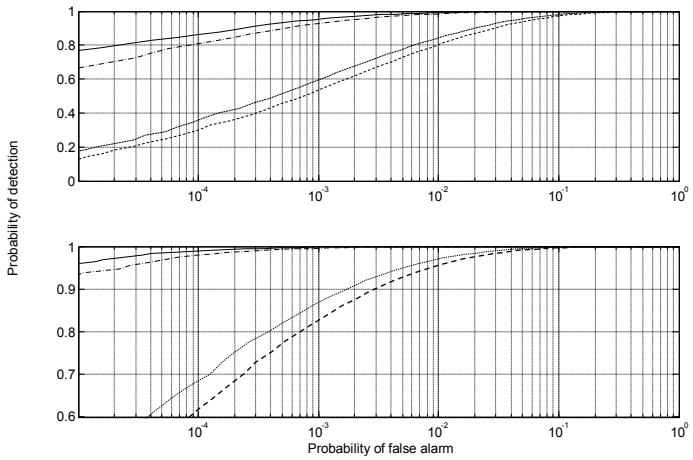

Figure 5: ROC curves comparisons for shot noise and ICCD detectors. The top graph contains the ROC curves for a signature content of 50. The continuous and alternated dashed curves are the results for the shot noise sensor for the matched filter and the ILIF detectors, respectively. The short dashed and long dashed curves are also respectively for the matched filter and for the ILIF detectors in the case of the ICCD sensor. The bottom plot has the same line code but it is the ROC curves for a signature content of 65.

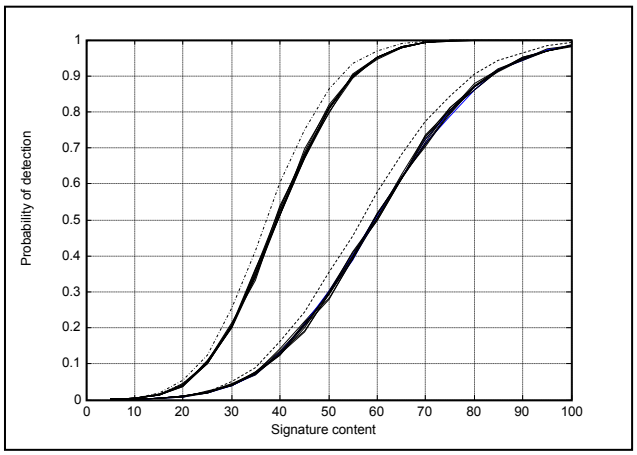

Figure 6: Probability of detection as function of the concentration for a probability of false alarm of 10^{-4}. The alternated dashed curve is the probability of detection as a function of signature content for the best result of the matched filter detector. The set of curves that are below set is the results of the ILIF detector for the different

signatures in the database. These curves are obtained with the shot noise signal. The dashed curve and the set of curves just below it are respectively for the best matched filter result and the ILIF in the case of ICCD sensor

5.2 Discussion for ROC curves

Figure 5 and 6 display an important advantage for the photon counter compared to the ICCD sensor. A much better sensitivity is displayed by photon counter, no matter what detector is used. The matched filter (MF) detector displays a small advantage over the ILIF detector in these conditions. It is true for the best case of signature MF detector. In some cases, when the distance between the assumed signature and the true signature is very large, the ILIF detector displays a better behavior than the MF detector. In most conditions, the detector using the 5^{th} signature has a behavior that is better or close to the ILIF detector. Therefore, if a signature represents the best compromise for the detection, it could be used to perform the detection with a better or equal performance compared to the ILIF detector. The complexity of the MF detector is however larger for the ILIF so the ILIF shall not be discarded. No correlation has been considered in the signal generation and processing. If it happened that correlation exists, it is possible that a matched filter presents a better performance. This remains to be studied. Note that correlation in the background arises from time variations of the background and that correlation consideration represents a much higher level of complexity, especially if it is adaptive. The ILIF and MF detectors cannot be used to perform a classification. The structure of the ILIF does not use signatures. For the MF detectors, the output value of the filter is a number which give information about the intensity of a signature contained in the signal. There is no way to tell which value is the best one using only that information.

5.3. Classification results

The confusion matrix displays the capability of a classifying method to discriminate the correct material from other materials susceptible to be present in a signal. We used three classification processes that are different implementations of adaptive matched filters. An operator or sequences of operators are computed and a selection method is required. To evaluate the capability of the classifications method, we used a closed set of signature. This mean that the signature used to simulate the signal is in the database used in the comparison of the signal. We used the same data to feed the three detectors. An example of a confusion matrix is provided in table 1:

Table 1: Example of a confusion matrix: The rows are the identification of the signature used to perform the simulations and the columns are the detected signature. The cells content are the probabilities that the classification provide the column signature. That matrix is for a background content of 100 and signature content of 100.

	1	2	3	4	5	6	7	8	9	10
1	0.660622	0.239335	0.085205	0.01367	0.00108	0.00007	0.00001	0	0	0
2	0.3411	0.32784	0.238812	0.07955	0.01166	0.00097	0.00006	0	0	0
3	0.110042	0.225085	0.336947	0.24034	0.07559	0.01109	0.00084	0.00005	0	0
4	0.02149	0.078997	0.22819	0.34678	0.24127	0.07222	0.01007	0.00089	0.00007	0
5	0.002695	0.014622	0.074727	0.23094	0.35579	0.23916	0.07076	0.01018	0.001	0.0001
6	0.000207	0.00167	0.012887	0.07224	0.23381	0.35863	0.23840	0.06981	0.01100	0.00131
7	1.50E-05	0.000125	0.001217	0.01123	0.06988	0.23778	0.35973	0.23539	0.07096	0.01363
8	2.50E-06	1.25E-05	9.00E-05	0.00105	0.01024	0.06925	0.23823	0.3592	0.23368	0.08823
9	0	0	5.00E-06	0.00004	0.00076	0.01009	0.06938	0.23880	0.35545	0.32545
10	0	0	0	0.00001	0.00004	0.00081	0.01011	0.07067	0.24095	0.67739

As an example from table 1, the probability to rightly classify signature 3 is 0.33695 and the probability to obtain signature 8 while signature 3 was used to perform the simulation is 0.00005. What can be seen is that for the edge signatures 1 and 10, the probability to accurately determine the contaminant is better than for the rest of the signatures. This can be attributed to the fact that these signatures only have one neighbor. The probability to accurately determine the right contaminant are very similar, however there seems to be a small increase with the signature index. This is probably due to the fact that the background signature is closer to the low index signature. Figure 7 displays a sequence

of results from the three detectors. The results look very different in structure. However, when subject to the same data, they provide the same results. Figure 8 shows the probability of right classification as a function of the signature content. The red curves correspond to the shot noise measurement while the blue curves are the results for the ICCD.

In figure 7, the plots of the first row are related to the shot noise sensor and the plots of the second row are for the ICCD sensor. The first plot to the left? is the LMS detector, ACE is the center plot and the matched filter is the plot to the right. The red plots are the results for the signature used in the simulation and the remaining lines are for the other signatures. The operators behave differently. The LMS detector plot the signature to be selected is the one giving the smallest value. FOR ACE and the matched filter the signature to be selected is the one giving the highest value. The three detectors look very different, however and surprisingly they give exactly the same classification results.

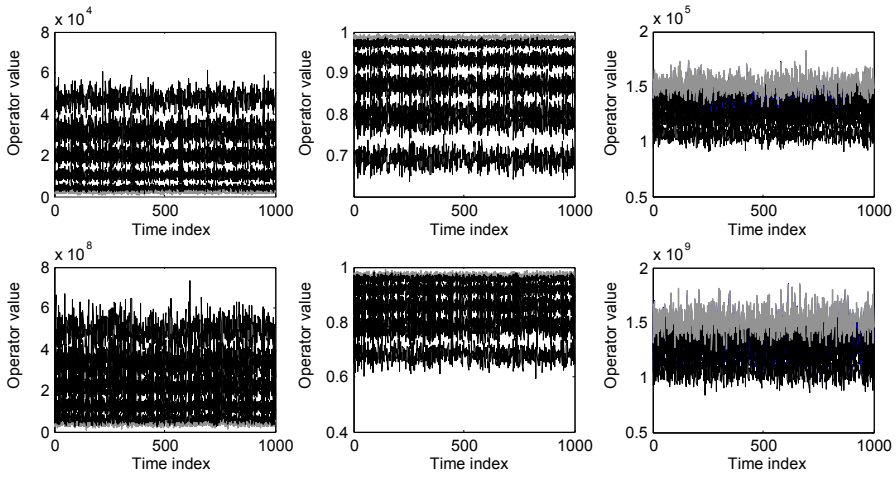

Figure 7: Sequence of results for from left to right LMS, ACE and AMF detectors for the case of shot noise in the graphs in the first row and for the ICCD in the second row. In each graph, the results are displayed for each signatures in the database. The wide grey curve is for the signature used in the simulation. The LMS classificator criterion is the smallest result and for the ACE, it is the result closest to 1 and for the AMF, it is the highest value.

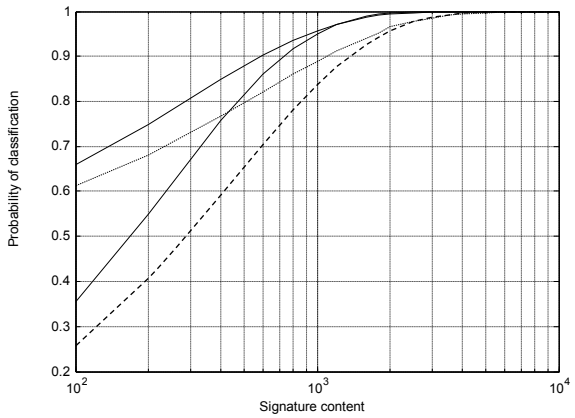

Figure 8: Probability of right classification for signature 1(curve set dashed and continuous lines above and the curve set (dashed and continuous) below.of the database as a function of signature content. The continuous curves are for the shot noise and the dashed curve for the ICCD noise. Signature 1 has an higher chance of being well classified.

Table 2: Confusion matrix for shot noise and signature content of 1000.

	1	2	3	4	5	6	7	8	9	10
1	0.95779	0.04220	0	0	0	0	0	0	0	0

2	0.04612	0.91834	0.03553	0	0	0	0	0	0	0
3	0	0.03748	0.93317	0.02935	0	0	0	0	0	0
4	0	0	0.03144	0.94305	0.02551	0	0	0	0	0
5	0	0	0	0.02641	0.95084	0.02274	0	0	0	0
6	0	0	0	0	0.02228	0.95589	0.02183	0	0	0
7	0	0	0	0	0	0.02084	0.95663	0.02253	0	0
8	0	0	0	0	0	0	0.02107	0.95455	0.02439	0
9	0	0	0	0	0	0	0	0.02249	0.95071	0.02679
10	0	0	0	0	0	0	0	0	0.02486	0.97514

Table 3: Confusion matrix for ICCD noise and signature content of 1000.

	1	2	3	4	5	6	7	8	9	10
1	0.88905	0.11089	0.00007	0	0	0	0	0	0	0
2	0.11691	0.78337	0.09969	0.00003	0	0	0	0	0	0
3	0.00021	0.10406	0.80474	0.09096	0.00004	0	0	0	0	0
4	0	8.00E-05	0.09344	0.82340	0.08307	0.00001	0	0	0	0
5	0	0	0.00004	0.08464	0.83659	0.07872	0.00002	0	0	0
6	0	0	0	0.00003	0.07831	0.84447	0.07719	0.00002	0	0
7	0	0	0	0	0	0.07591	0.84614	0.07791	0.00003	0
8	0	0	0	0	0	0.00002	0.07572	0.84338	0.08086	0.00002
9	0	0	0	0	0	0	0	0.07793	0.83533	0.08674
10	0	0	0	0	0	0	0	0	0.08208	0.91792

Table 4: Confusion matrix for ICCD noise and signature content of 2000.

	1	2	3	4	5	6	7	8	9	10
1	0.964977	0.035022	0	0	0	0	0	0	0	0
2	0.043175	0.92491	0.031915	0	0	0	0	0	0	0
3	0	0.035092	0.938577	0.02633	0	0	0	0	0	0
4	0	0	0.02862	0.94899	0.02238	0	0	0	0	0
5	0	0	0	0.02337	0.95614	0.02048	0	0	0	0
6	0	0	0	0	0.02010	0.96033	0.01956	0	0	0
7	0	0	0	0	0	0.01862	0.96161	0.01976	0	0
8	0	0	0	0	0	0	0.01860	0.95997	0.02142	0
9	0	0	0	0	0	0	0	0.02000	0.95596	0.02403
10	0	0	0	0	0	0	0	0	0.02053	0.97947

There is no difference in the results obtained from a detector (AMF, LMS or ACE) in the context of noise dependency with the intensity of the signal. The authors do not understand why. The type of sensor (photon counter or ICCD) however has an impact of approximately a factor of 2 in ability to classify correctly. To obtain similar probabilities of classification, the signature content needs to be higher by a factor of 2 for the ICCD sensor. This means that the concentration in aerosol needs to be two times higher. For a probability of classification above 0.99, the signature content should be above 2000 for the photon counter sensor and 4000 for the ICCD sensor. The probability of error in the classification depends on the distance of a signature and of its competitor and as the signal levels are increased the

classification performance increases. The closer two signatures are the more chances classification gets an error between the two.

6. Conclusion

In this study we compared the advantages provided by a photon counter sensor over an ICCD sensor for the spectral detection and classification of fluorescent material. We first described a signal model for both sensors encompassing a stationary background, particular set of signature and random signal generation. We then introduced some algorithms, for detection and classification of the material. Monte Carlo simulations have been performed to compare the capabilities of the sensors and of the detection algorithms. The Photon Counter sensor displayed a net improvement in performance for both detection and classification. The detection operation shows an increase in performance of approximately 1.5 in signature content for a false alarm probability of 10^{-4} for the photon counter sensor. In the case of the classification, the increase in performance is approximately a factor of 2 in signature content, which mean that the shot noise detector is able to classify materials having a concentration that is 2 times lower than the ICCD. In the case of the operators used to perform detection, the adaptive detectors display a better performance than the integrated signal at a price of higher complexity. The increase in performance is very small. In the case of the adaptive classifiers operators: ACE, AMF, ALS the performance are exactly the same but the reason for that are not understood yet and it remains to be studied. The noise model: no correlation between bands and a noise increase with the signal can account for that.

No filters have been used in this study. The bands are decorrelated and filters are often used in multivariate processing to remove the correlation in the background. There could be filters specifically adapted to multivariate Poisson distributed data or for ICCD generated data, but there design is devoted to future work. Time varying backgrounds have not been studied. In many cases when a sensor is staring at a given location with a very small signal, the acquisition of a set having a sufficient size to enable the estimation of a covariance matrix accounting for the time variations may represent a daunting task.

Another problem that we have not studied is the estimation of the thresholds. In a practical system the data will slowly enter the system; it is especially true for the ICCD sensors. An interesting approach is to use adaptive thresholds to maintain the false alarm rate at a given level. A threshold estimation method needs to be designed with consideration of the background data. A number of samples need to be acquired to estimate the threshold. The time variations of the background and its statistics, mainly the variance determines the number of samples that is required. The resulting method will be obtained from a compromise between the mathematical requirements and a system capability. Static thresholds cannot guarantee a specific level of false alarm probability in all cases.

7. Reference:

[1] Teranishi N., “Required conditions for photon-counting image sensors”, IEEE transactions on electron devices, vol. 59, No. 8, August 2012.

[2] Sandel B.R., Broadfoot A.L. “Statistical performance of the intensified charged coupled device”, Applied Optics, Vol. 25, No. 22, November 1986.

[3] Robey F.C., Kelly E.J., Nitzberg R., “A CFAR Adaptive matched filter detector”, IEEE Transactions on aerospace and electronic systems, Vol. 28, no 1, January 1992, PP. 208-216

[4] Scharf L., McWhorter L.T., “Adaptive matched subspace detectors and adaptive coherence estimators”, Prof Asilomar Conf. on signals, systems and computer, November 1996.

[5] E.J. Kelly, “An adaptive detection algorithm”, IEEE Transactions on aerospace and electronic system, vol. AES 22, no1, March 1986,PP. 115-127

[6] Laflamme C., Simard J.R., Buteau, S., Lahaie P., Nadeau D., Houle O., MathieuP., Dery B., Roy G., Ho J., Duchaine C., “Effect of growth media and washing on the spectral signatures of aerosolized biological simulants”, Applied Optics, Vol. 50, Issue 6, PP. 788-796, 2011

[7] Hill S.C., Pinnick R.G., Niles S., Garvey, D.M., Pan Y., Holler S., Chang R.K., Bottiger J., Bronk B.V., Chen B.T., Orr C., Feather G., "Real-Time measurement of fluorescence spectra from single airborne biological particles", Field analytical chemistry and technology, vol. 3 no. (4–5), PP.. 221–239, 1999